JOURNAL OF AIRCRAFT
Vol. 37, No. 3, May–June 2000

Wind-Tunnel Tests of a High Lift Generation and Stall/Spin Recovery System

D. K. Nowak*
Micron Corporation, Winchester, Tennessee 37398-4526
and
U. P. Solies†
University of Tennessee Space Institute, Tullahoma, Tennessee 37388-9700

A novel aerodynamic flight control system, called the delta flap, for the generation of high lift and recovery from stall and spin was studied in wind-tunnel tests. A limited matrix of configuration parameters, angles of attack, and Reynolds numbers were investigated. The delta flap system consists of one or more slender delta-shaped flaps with a chord length typically less than one-third of the aircraft wing chord that are deployed close to the leading edge above the wing. The results of the study indicate that the delta flap, deployed in a proper configuration prior to stall, makes an aircraft wing virtually stall proof. Water-tunnel tests have also shown that deployment of the delta flap at poststall angles of attack reverses flow separation over the aircraft wing. Finally, wind-tunnel tests have proven that the delta flap significantly increases the maximum lift coefficient of the wing and reduces or reverses the nose-down pitching moment.

Nomenclature

A = wing aspect ratio, b/c
A_f = delta flap aspect ratio, $4\tan(\varphi/2)$
b = wing span
b_f = delta flap span
C_D = drag coefficient
C_L = lift coefficient
C_m = pitching moment coefficient
c = wing chord
c_f = delta flap chord
$\overline{c_f}$ = delta flap chord ratio, c_f/c
c_{sf} = split flap chord
$\overline{c_{sf}}$ = split flap chord ratio, c_{sf}/c
d_f = spanwise distance between delta flap centerlines
$\overline{d_f}$ = nondimensional spanwise delta flap spacing, d_f/b_f
h_f = delta flap height, distance between wing upper surface and delta flap trailing edge
$\overline{h_f}$ = relative height of delta flap, h_f/c
i = delta flap incidence angle
x_f = chordwise delta flap position, that is, distance of delta flap trailing edge behind wing leading edge
$\overline{x_f}$ = chordwise relative position of delta flap, x_f/c
α = wing angle of attack
δ = split flap deflection angle
φ = delta flap apex angle

Introduction

THE delta flap[1] is a novel aerodynamic flight control system for the generation of high lift and for stall/spin recovery of aircraft which was studied with respect to its application to general aviation aircraft. If designed for asymmetrical deployment, it may serve as a control for roll and yaw moment. If deployed in a symmetric configuration, it increases lift and facilitates recovery from stall. The main objective of the feasibility study was to show that a model wing, with the delta flap deployed, allowed higher angles of attack, without the occurrence of flow separation, than the same wing without delta flap deployment and that the maximum C_L obtained with the delta flap deployed was higher than that for the wing without the delta flap. Therefore, flow-visualization tests in a water tunnel were performed, as well as measurements of C_L, C_D, and C_m of the model wing in a wind tunnel. Also, flight tests were conducted with a remotely controlled model aircraft, equipped with delta flaps. A common airfoil was used for all tests. The scope of this paper is limited to the wind-tunnel studies. Water-tunnel test results are documented in Ref. 2. Flight test results with a model aircraft will be published separately.

Description of the Delta Flap

Figure 1 is a conceptual illustration of the delta flap system. Typically, the delta flaps have a maximum chord of approximately $\frac{1}{4}$–$\frac{1}{3}$ of the aircraft wing chord and an aspect ratio between 1 and 2. The airfoil section of the delta may be a thin lens shape with sharp leading edges or simply a sharp-edged flat plate. The delta flaps are shown in a deployed state. In this application, each delta flap rests on three levers, one each at the tips and one at the apex of the delta. Figure 2 shows how, during deployment, these levers rotate around specific points within the aircraft wing thereby lifting the delta flap above the aircraft wing surface to a specific position and angle. During deployment the vertical plane of symmetry of the delta flap remains parallel to the aircraft plane of symmetry. The illustrated deployment system demonstrates the mechanic feasibility of the concept and is only one example of many conceivable ways to deploy the delta flap. Design studies of practical ways to deploy the delta flap, compatible with modern wing designs, are subject to future research.

The deployed delta flap must be positioned such that it protrudes outside the boundary layer or any area of flow separation into the healthy, high-energy airflow surrounding the aircraft wing. Therefore, the delta flap is positioned above the upper aircraft wing surface at a positive incidence angle to the aircraft wing chord. As indicated in Fig. 2, the position of the delta flap relative to the chord line of the wing can be changed depending on the flight condition of the aircraft. During cruise flight, for example, the delta flaps can be retracted such that they become part of the upper wing surface. During approach to landing, stall and spin recovery, or other flight maneuvers requiring delta flap deployment, a lever mechanism lifts the delta flap above the aircraft wing surface while simultaneously moving it toward the leading edge and setting the angle of incidence. The mode of operation during various flight conditions and

Received 21 June 1999; revision received 10 November 1999; accepted for publication 16 November 1999.

*President, Route 2, Box 271A, Orchard Lane.
†Associate Professor, Mail Stop 20, Aviation Systems and Aerospace Engineering. Member AIAA.

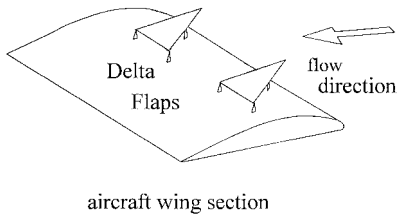

Fig. 1 Conceptual illustration of the delta flap.

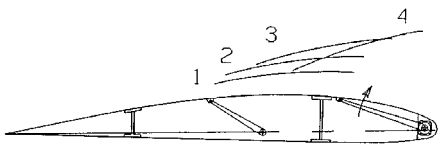

Fig. 2 Wing section with typical sequence of delta flap positions during deployment.

the optimum position of the flap for each flight condition are subject to future research.

Test Objectives

The research objectives of the wind-tunnel tests were as follows.

1) Determine the aerodynamic coefficients C_L, C_D, and C_m, as a function of angle of attack α for the plain wing (baseline).

2) Determine the aerodynamic coefficients for the same wing under identical flow conditions but with delta flaps deployed.

3) Compare the results and show the effect of the delta flaps on lift, drag, and pitching moment. Of particular interest were maximum lift and angle of attack for maximum lift.

4) Determine the flow separation characteristics of the wing, using tufts attached to the wing surface for flow visualization.

5) Determine the effect of the delta flaps on the flow separation characteristics, such as changes of flow patterns during stall progression and delay of flow separation to higher angles of attack.

6) Determine Reynolds number effects by measuring the aerodynamic coefficients at different air velocities.

7) Determine the effects of delta flap geometry, such as flap position, incidence angle, and aspect ratio, on the aerodynamic coefficients.

The wind-tunnel tests were not meant to produce an optimum delta flap configuration, but rather to establish trends and affirm that these trends were typical.

Wind-Tunnel Test Facility

The University of Tennessee Space Institute's (UTSI) wind tunnel used for this study was a draw through open system. It had an enclosed 35.6 × 50.8 cm test section and an overall length of 15 m. A 1.22-m-diam. fan was located near the tunnel exit and was driven by a 56-kW electric motor with variable speed control. The tunnel could generate airflow velocities in excess of 60 m/s, corresponding to Reynolds numbers of 4.1×10^6 per meter of reference length.

The test wing was mounted horizontally in the test chamber and rotated about a shaft that penetrated a side wall. The shaft doubled as a strain-gauge force balance for the measurement of normal and side force components and torque (see Fig. 3). The signals from the strain-gauge bridges were supplied to a personal computer-based data acquisition system. A program controlled the number of samples per measurement and contained a data reduction routine that converted the signals to aerodynamic coefficients, C_L, C_D, and C_m.

The force balance was attached to an index head that allowed 360-deg variation of the angle of attack with an accuracy of 0.01 deg. The index head also served as conduit for signal wires from the strain gauges.

Air velocity was determined with a dynamic pressure probe in the test section entrance. The U-tube manometer used for the pressure readout was calibrated in inches and had a slanted tube for pressures below 2 in. (5.08 cm) of water and a vertical tube for pressures above that value. This resulted in a 0.01-in. (0.25-mm) resolution below

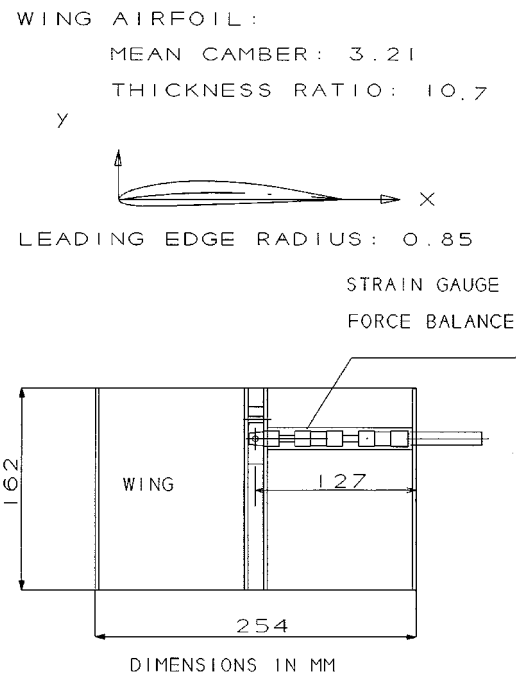

Fig. 3 Wind-tunnel model of the wing with internal force balance.

the 2-in. mark, and a 0.1-in. (2.54-mm) resolution above the 2-in. mark. The side wall opposite to the index head was transparent, permitting observation of the test article and airflow patterns.

Wind-Tunnel Model

Wing

Constraints on time and resources permitted the production of only one wing model, which was tested with different flaps and deployment configurations. The choice of the wing geometry was made for practical reasons, that is, ease of construction, compatibility with the airplane model, rather than for optimum compatibility with delta flaps, or for particular airfoil characteristics. The chosen airfoil was adopted from a high-speed model airplane. The airfoil combined low drag and an almost flat bottom surface with a relatively sharp stall break. Typical Reynolds numbers for this application range approximately from 6×10^4 to 1×10^6.

The wing had a rectangular planform with the airfoil section shown in Fig. 3 and Table 1. The airfoil contours were made smooth and kept within 1 mm of the listed coordinates. The nature of this research did not warrant precision machining or similar costly measures.

The wing model was built up from 38-mm-wide solid wood sections, which were individually shaped using metal templets of the airfoil as reference and then lined up on two threaded compression rods and glued and bolted together to form the complete wing. The wing surface was coated with epoxy, sanded, and then painted with epoxy paint. In this form, the wing model was used for water-tunnel tests.

The wing model used in the wind-tunnel was obtained by modifying the water-tunnel model for internal mounting of the force balance. The wooden wing was cut at the location of the attachment point of the balance, and a metal section with a conical attachment for the balance was fabricated and mounted into the wing. A channel for the balance was opened toward the wing root, and a 0.3-mm sheet aluminum cover was glued to the upper and lower wing surface to give the wing model stiffness and structural integrity to withstand the aerodynamic loads in the wind tunnel, which were considerably higher than in the water tunnel.

The span of the wing and the thickness of the profile were dictated by the dimension of the available balance. The attachment point between the wing and the force balance was a conical press fit, located at the airfoil quarter chord and a spanwise distance of

Table 1 Airfoil coordinates (in percent of chord)

Lower surface		Upper surface	
X	*Y*	*X*	*Y*
0.54	1.13	0.58	−1.11
1.41	1.90	1.53	−1.62
2.85	2.82	2.33	−1.93
4.92	3.74	3.76	−2.24
7.09	4.46	5.73	−2.54
9.42	5.12	7.79	−2.80
12.61	5.85	11.37	−3.00
17.12	6.73	17.10	−2.97
22.65	7.43	22.96	−2.81
34.32	8.26	28.37	−2.63
36.92	8.26	34.16	−2.41
40.11	8.22	40.00	−2.21
45.80	8.07	45.59	−2.01
51.40	7.77	51.26	−1.80
56.83	7.30	56.62	−1.58
62.68	6.65	62.42	−1.35
68.19	5.91	68.08	−1.18
73.76	5.01	73.92	−0.95
79.66	3.89	79.46	−0.75
85.20	2.86	85.05	−0.55
90.70	1.82	90.55	−0.35
96.14	0.79	96.09	−0.13
100.00	0.06	100.00	0.00

127 mm from the wing root. The wing span was chosen such that the attachment point of the balance was close to the aerodynamic center of pressure. The balance had a maximum diameter of 12.5 mm and was mounted inside the wing. It required enough clearance to prevent it from touching the wing structure under aerodynamic load conditions (fouling). Therefore, the maximum airfoil thickness was chosen as 13.5 mm. Load tests confirmed that there was no fouling. Figure 3 shows the rectangular wing with a chord $c = 162$ mm and a half span $b/2 = 254$ mm. The corresponding full span aspect ratio was $A = 3.14$.

The gap between the wing root and the wind-tunnel wall was kept at less than 1 mm. This was a compromise between the conflicting desires of reducing airflow through the gap and providing sufficient clearance for wing vibration during conditions of separated flow. Initial attempts to seal the gap with foam rubber resulted in erroneous force readings and were abandoned.

Delta Flaps

Three different aspect ratio flaps were used: $A_f = 1$, 1.5, and 2.0. The generic flap design is shown in Fig. 4. The flaps were constructed from 0.5-mm sheet aluminum. The leading edges were sharpened. Each flap was reinforced by a smaller delta-shaped aluminum plate that was glued to the bottom of the flap. In addition, in case the glue failed, wire fasteners were used to keep the reinforcement plate fastened to the delta flap during the tests.

The delta flaps were attached to the wing by struts, made from sheet aluminum. The struts were attached to the flap by wire bearings and to the wing by glue. The struts could rotate around the bearings. Therefore, the angle of attack could be changed between runs by opening the glue attachment at the leading edge of the wing and raising the apex strut. The delta flap position on the wing surface could be changed by removing the whole delta flap assembly from the wing surface and gluing it to a different location. For a change in height above the wing surface, the trailing edge strut of the delta flap was replaced by a longer strut. For different aspect ratios, different flap assemblies were built.

Split Flap

Part of the testing required a split flap extending from the wing airfoil. To simulate a model split flap, a sheet metal strip of approximately 5 cm. width was bent at its centerline to approximately 60 deg and glued to the underside of the wing near its trailing edge. Later in the testing, the bending angle was reduced to approximately

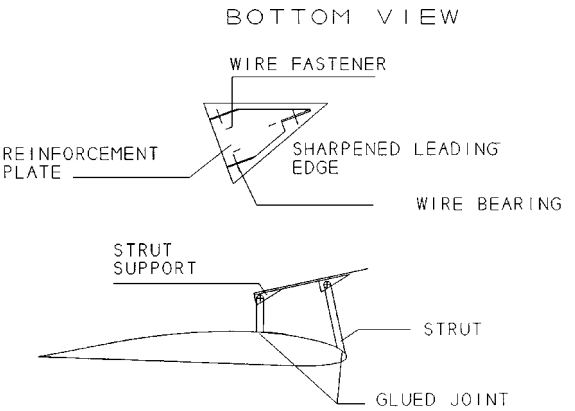

Fig. 4 Model delta flap assembly.

30 deg. The exact flap deflection angles were measured with respect to the airfoil chord line and are shown in the configuration graphs.

Test Procedures

At the start of the test program, the balance was calibrated. The resulting gauge constants and effective locations of the strain-gauge bridges were entered as parameters into the data reduction routine. The procedure was repeated at about midprogram, when a new, more sensitive, force balance was installed. Also, before the first test run and after every major wing modification, a tare calibration was performed to permit correction of the data for the weight of the wing model. Again, the tare data and appropriate correction equations were entered into the data reduction routine. At the beginning and at the end of each test run, readings at zero tunnel speed and zero angle of attack were taken, to confirm the proper function and calibration of the equipment.

Each test run consisted of a series of measurements taken at constant tunnel speeds and a range of angle of attack settings, typically from −4 to 30 deg and above. Angle-of-attack increments were typically chosen as 4 deg in the linear range of the lift curve ($\alpha < 16$ deg) and reduced to 1 deg in the nonlinear range ($\alpha > 16$ deg). To eliminate random scatter, the data reduction program took several readings at each angle of attack setting, and calculated the root mean square, which was taken as a representative value for this condition. The number of samples was increased in the nonlinear range, where the onset of flow separation caused some wing vibration and increased scatter of the data. At the end of each run, the data set was plotted for evaluation, and a decision for the parameter changes for the next test run was made. Each change of configuration required a modification of the wing assembly between tests because the flaps were permanently fixed to the wing. To account for any changes in the model, baseline tests were periodically repeated.

A total of 66 test runs with 29 configurations of delta flaps were performed, including several runs with a split flap. Tunnel speed selections ranged from 15.2 to 53.3 m/s. Each test run was a complete sweep of angles of attack. The delta flaps were fixed in position throughout the whole test run. The parameters that were changed between runs were aspect ratio, flap position, flap attitude, flap distribution over the wing span, and/or Reynolds number. Variables describing the geometric parameters of different configurations are defined in the Nomenclature and shown in Fig. 5. The number of configurations was necessarily limited and was chosen as a first step to demonstrate the feasibility of the delta flap. Optimized delta flap geometries and positions, including optimum positions during flap extension and interaction with different airfoils, are subject to future research.

Results and Discussion

Figure 6 represents a typical result of a test run of a configuration with three delta flaps compared to the baseline wing. Some general findings are described first, followed by a discussion of selected examples.

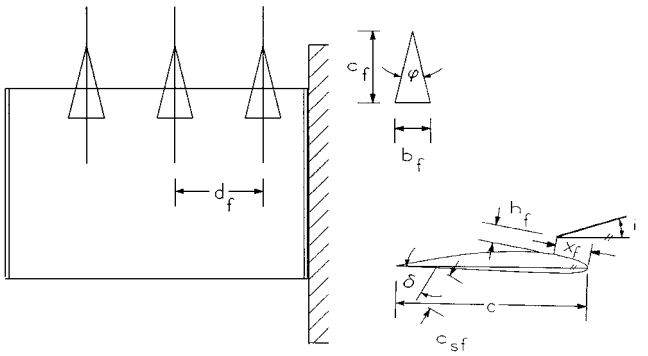

Fig. 5 Geometric parameters defining the delta flap configuration.

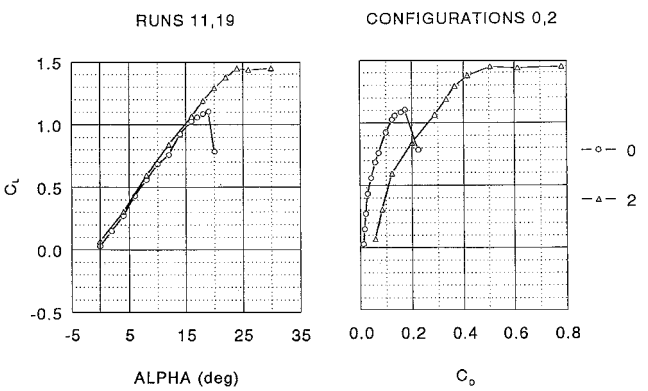

Fig. 6 Typical result of wind-tunnel test.

Maximum Lift and Stall

The measurement of the aerodynamic coefficients showed that proper deployment of the delta flap increased the maximum lift coefficient of the plain wing by extending the lift curve to higher angles of attack and then maintained high values of the lift coefficient over a wide range of wing angles of attack. The sharp stall break of the basic wing was eliminated. For the delta flap wing configuration, there was no clearly defined stall angle that could be associated with a sudden loss of lift.

Drag

The delta flap wing configuration produced higher drag than the plain wing. The drag increase depended strongly on the incidence angle of the delta flap. Generally, higher incidence angle caused higher drag and higher maximum lift. The data indicate that proper selection of the delta flap incidence will permit optimization of the configuration for a desired lift to drag ratio, for example, a small reduction in incidence angle can provide a significant drag reduction, while the maximum lift is only slightly reduced.

Pitching Moment

The pitching moment coefficient of the basic wing remained at a constant negative value for angles of attack up to the stall. This result was expected because the force balance was installed at the quarter chord and the airfoil had a positive camber causing a pitch-down moment (negative). The delta flaps contributed a moderate pitch-up moment, slightly reducing the negative moment of the plain wing or, in some cases, changing it to a positive moment. At the stall angle, the plain wing experienced a sharp drop in C_m, whereas the C_m of the delta flap wing dropped only gradually and experienced much less change.

Flow Visualization

Tufts attached to the upper surface of the wing indicated that the flow over the plain wing started to separate from portions of the upper wing surface at about 16-deg angle of attack. Further increase of the angle of attack (>18 deg) resulted in fully separated flow, with areas of flow reversal and large eddy turbulence. This behavior coincided with a sudden drop of the lift coefficient. For the wing with delta flaps, the flow remained attached to the upper surface downstream of the delta flaps for practically all wing angles of attack that were tested (−4–45 deg). At higher angles of attack (>20 deg), leading-edge flow separation bubbles were indicated by the tufts, but the flow reattached farther downstream and remained attached up to the trailing edge. The lift coefficients increased well beyond the baseline wing stall angle of attack and then gradually leveled off between 20- and 24-deg angle of attack for most of the flap configurations tested. No corresponding change in the surface flow pattern could be observed.

Reynolds Number Effects

For the plain wing, an increase in Reynolds number *Re* slightly increased the maximum lift coefficient and caused a more pronounced decrease in drag coefficient. For the delta flap wing configuration, the change of aerodynamic coefficients due to Reynolds number was small. From observations of the tufts on the wing surface, it appeared that the flow became more stable and more strictly organized as the Reynolds number increased. This observation was also supported by a reduction of the poststall wing vibration. Comparing water-tunnel and wind-tunnel tests, however, the Reynolds number effects on visible flow reattachment were significant. Whereas the water tunnel tests (Reynolds number up to 4×10^4) showed a distinct maximum angle of attack up to which the flow could be kept attached to the upper surface by delta flaps, the flow in the wind tunnel (Reynolds number up to 5.9×10^5) could be kept attached throughout the whole tested range of angles of attack by proper positioning of the delta flaps.

Wind-Tunnel Wall Effects

Because of the large wing model size (16.2 cm chord length) relative to the wind-tunnel test section (35.6 cm height), a certain amount of blockage affected the data at very high angles of attack. Whereas this effect puts into question the absolute values of some of the poststall lift data, the relative differences between the basic wing and the delta flap wing configuration are properly documented and valid. This type of result was the main thrust of this research.

Force Balance Sensitivity

Runs 1–39 were accomplished with a 130-N force balance with symmetrical sections for normal and side force components. At low tunnel speeds, the drag forces routinely remained below 4 N, causing a relatively weak signal. Therefore, the low Reynolds number data were somewhat scattered. These data sets are still valuable in showing trends. For runs 40–66, a more sensitive, asymmetrical force balance was used with a 90-N range for normal forces (lift) and a 20-N range for side forces (drag). This balance also had a torque section, permitting measurement of wing pitching moments. Consequently, the data obtained with this balance had improved quality.

Selected Parameter Variations

Figures 7a–7d show a selection of the configurations tested. Figure 6 and Figs. 8–14 compare specific wind-tunnel runs to indicate trends of the effect of delta flap parameters on coefficients of lift, drag, and pitching moment. Again, note that this research was exploratory in nature and not a systematic parameter variation for optimization purposes. Complete test results can be found in Ref. 2.

Effect of Flap Number Variation

Figure 8 shows a comparison of runs with three, two, and one delta flaps (configurations 2, 3, and 4), and the baseline wing (configuration 0). Although there is some data scatter in the poststall region, the data clearly show the effect of delta flaps on lift increase and elimination of the sharp stall break in the baseline data. Whereas the three-flap configuration shows the highest maximum lift coefficient and the smoothest transition from the sloped lift curve to

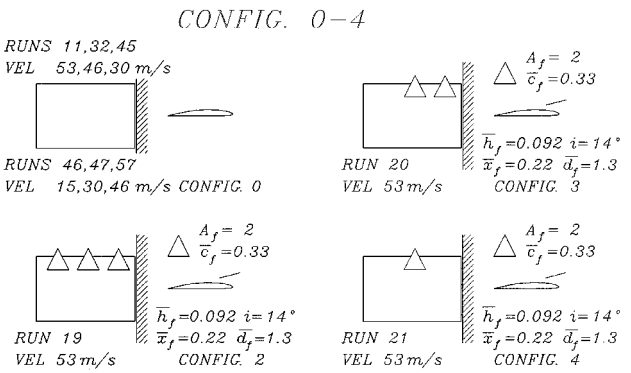

Fig. 7a Selection of delta flap configurations tested: 0–4.

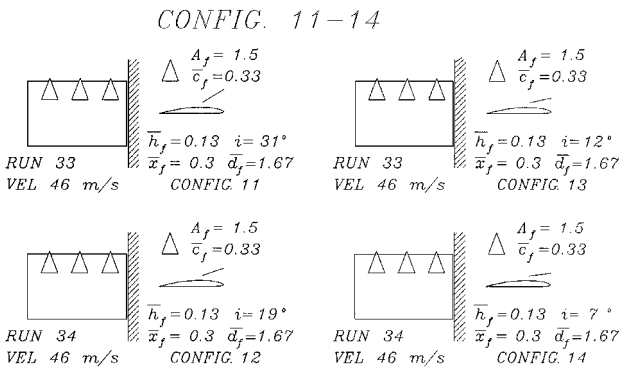

Fig. 7b Selection of delta flap configurations tested: 11–14.

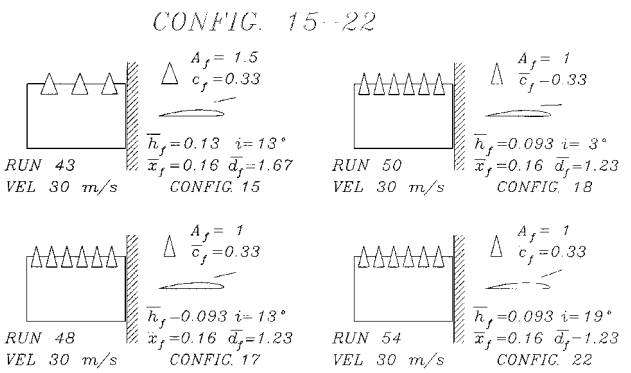

Fig. 7c Selection of delta flap configurations tested: 15–22.

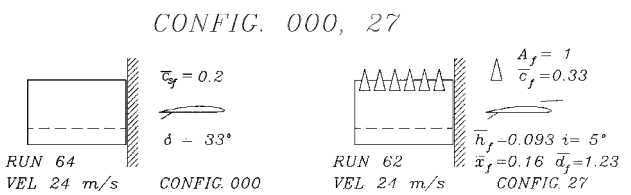

Fig. 7d Selection of delta flap configurations tested: 000 and 27.

the level part, all lift curves for the flapped configurations are surprisingly close together. This result shows that the lift effect of a single flap is much greater than one-third of the combined effect from three flaps in the tested configuration, indicating the significant spanwise spreading of the flap-induced flow improvements and the corresponding large influence of a single flap. The drag, however, increases at approximately equal increments with each additional flap. These observations point toward a possibly more optimal configuration with a larger spanwise spacing of the flaps.

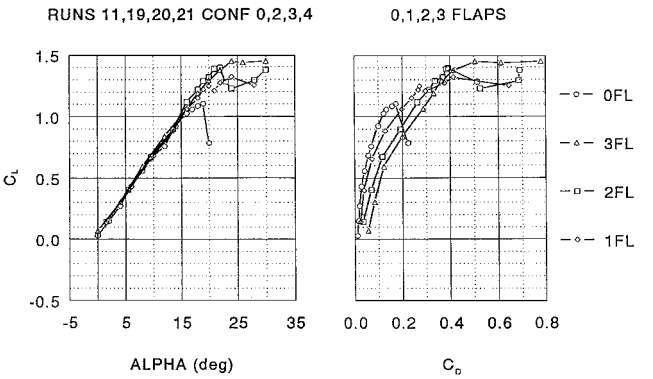

Fig. 8 Effect of number of delta flaps.

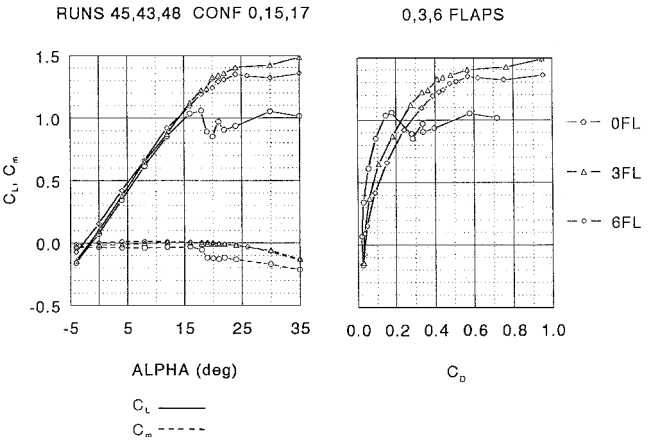

Fig. 9 Effect of delta flap spacing and aspect ratio.

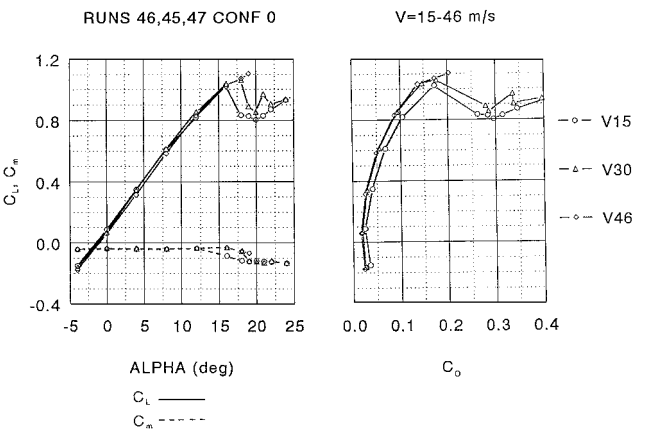

Fig. 10 Effect of Reynolds number on basic airfoil.

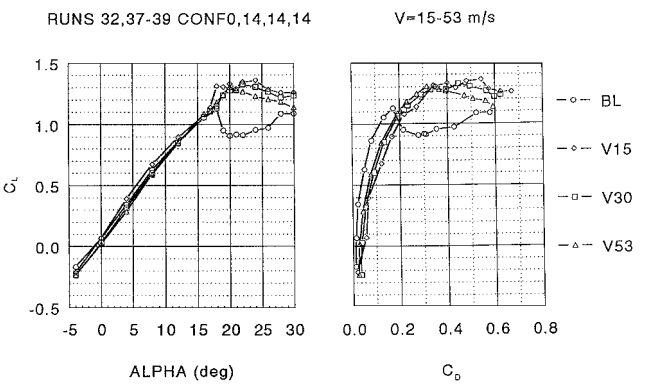

Fig. 11 Effect of Reynolds number.

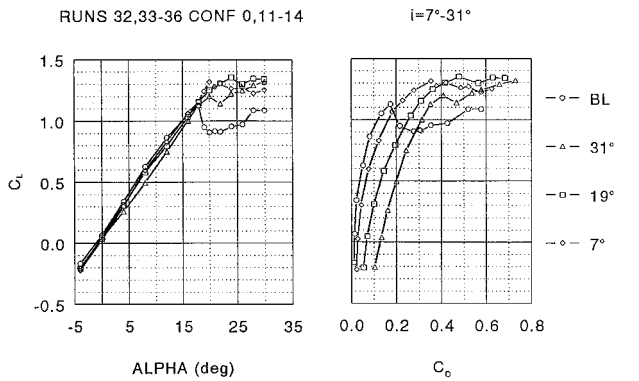

Fig. 12 Effect of delta flap incidence (configuration 11, three flaps).

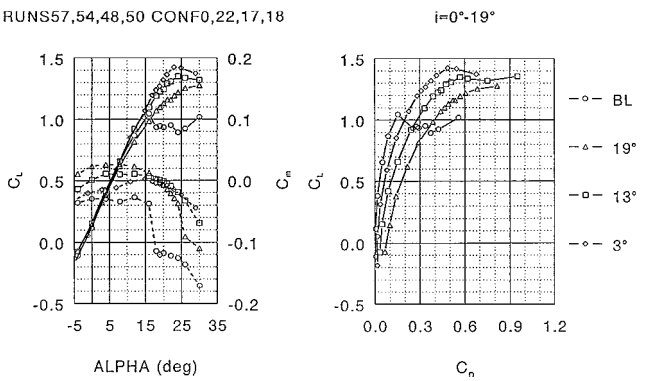

Fig. 13 Effect of delta flap incidence (configuration 17, six flaps).

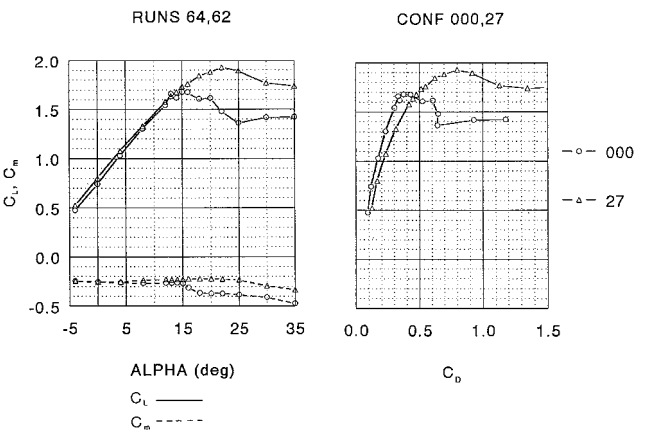

Fig. 14 Effect of delta flaps on split flap configuration.

Effect of Flap Spacing and Aspect Ratio Change

Figure 9 shows the comparison of three widely spaced flaps of aspect ratio 1.5 (configuration 15), with six closely spaced flaps of aspect ratio 1 (configuration 17), and the baseline (configuration 0). Again, the lift curves are close together, indicating that the flap effects are not very sensitive to flap spacing and aspect ratio for the tested configurations. The three flaps with higher aspect ratio and wider spacing are preferable because they have less drag and provide more lift. Figure 9 also shows the flap effect on pitching moment: The sudden drop of the baseline near 18-deg angle of attack is replaced by a gradual decline starting near 24-deg angle of attack.

Effect of Reynolds Number Change

Figure 10 shows α sweeps of the baseline wing at wind-tunnel speeds of 15.2, 30.5, and 45.7 m/s, corresponding to wing chord Reynolds numbers of 0.17, 0.34, and 0.51×10^6. The higher Reynolds number runs yield delayed stall and increased values of the maximum lift coefficient, while the drag coefficients decrease with increasing Reynolds number. Both phenomena are caused by boundary-layer effects and are generally well understood.[3] Figure 11 shows the three-flap configuration 14 at tunnel speeds of 15.2, 30.5, and 53.3 m/s, corresponding to wing chord Reynolds numbers of 0.17, 0.34, and 0.59×10^6. The effects on lift and drag are small, with both, lift and drag coefficients tending to decrease slightly with increasing Reynolds number.

Effect of Delta Flap Incidence Variation

Figure 12 shows the effect of incidence change on the three-flap configuration 11. A very large flap incidence of 31 deg results in a reduction of lift below the baseline before stall ($0 < \alpha < 16$ deg) and the lowest $C_{L\max}$ of the tested incidence angles. This configuration also causes the highest drag. The 19-deg flap configuration yields the maximum lift coefficient. Subsequent lower angle settings of 12 deg (not shown) and 7 deg yield slightly lower lift, but significantly lower drag. The maximum lift coefficient is not very sensitive to delta flap incidence changes in this range, while the drag coefficient is significantly affected. Figure 13 shows the effect of incidence change on the six-flap configuration 17. Here, a 3-deg flap incidence angle yields the maximum lift coefficient and relatively low drag.

Effect of Delta Flaps on Split Flap Configuration

Figure 14 shows typical α sweeps of a six-delta-flap-plus-split-flap configuration versus the split-flap-only configuration. The effect of the delta flaps is very similar as on the basic airfoil: smoothing of the stall break and increasing of maximum lift.

Conclusions

This research established a number of unique properties of the delta flap. Although only one airfoil and one wing geometry was tested, the nature of the delta flap and the related flow mechanisms indicate that these properties are most likely universal, applicable to many airfoils and wing geometries.

The deployment of the delta flaps radically improves the stall characteristic of a wing in a controlled and predictable way. This altered flow behavior opens the possibility to use wing geometries and airfoils in aircraft design that, for example, provide excellent cruise performance but are not very safe to fly during landing and takeoff because of poor stall characteristics. In addition, permanent fixtures for stall improvement, such as wing twist, boundary-layer fences, vortex generators, stall strips, etc., may be eliminated.

The ability to reverse flow separation is one of the most significant features of the delta flap. Water-tunnel tests,[2] during which the delta flap was deployed after the flow over the wing had fully separated, indicated the possibility to recover quickly from stall and spin. The property of the delta flap to facilitate flow recovery makes the delta flap a unique safety device. Another important safety feature is that the delta flap, after reaching $C_{L\max}$, maintains lift coefficients close to $C_{L\max}$ for a wide range of angles of attack, thus preventing rapid loss of lift (stall) or, worse, asymmetric loss of lift (departure) that initiates aircraft spin. This property of the delta flap makes the aircraft very stable and safe to fly during flight phases that are traditionally prone to pilot error, namely, takeoff and approach to landing.

An additional feature is the positive change of the pitching moment of the wing when the delta flap is deployed. Conventional flaps cause strong negative pitching moments, which typically have to be balanced by a negative lift force on the horizontal tail. This increases the stall speed of the aircraft, adds trim drag, and drives the design to larger required areas for tail and wing, increasing weight and drag. The positive (pitch-up) moment generated by the delta flap has a favorable effect on these components.

Previously conducted flow-visualization tests[2] revealed the three dimensionality of the flow in the vicinity of the delta flap and showed that its area of influence is roughly the extension of the leading edge of the delta flap in the downstream direction. Because of entrainment effects, upstream streamlines converge on the delta flap, giving the flap the appearance of a flow energy collector. This makes the flap very efficient for its size, with the promise of significant weight savings over conventional flap systems.

Whereas the tufts on the upper surface of the delta flap wing indicated no flow separation for all tested angles of attack, the lift coefficients leveled off typically near 24-deg angle of attack. The exact flow mechanisms causing this, as well as corresponding optimizations of the delta flap geometries, remain subject to future research.

Acknowledgments

This feasibility study of the delta flap was conducted under NASA Contract NAS1-98081 (see Ref. 2). The authors express their gratitude for the support of this research by NASA Langley Research Center and the guidance by Paul Stough, who served as the Contract Monitor.

References

[1]Nowak, D. K., "Aircraft Wing Flaps," U.S Patent 5,772,155, 30 June 1998.

[2]Nowak, D. K., and Solies, U. P., "A High Lift Generation and Stall/Spin Recovery System," NASA CR NAS1-98081, 1998.

[3]Abbott, I. H., and von Doehnhoff, A. E., *Theory of Wing Sections*, Dover, New York, 1959, pp. 137, 148.